Journal of Applied Sciences

ISSN 1812-5654

science alert

ANSInet
an open access publisher
http://ansinet.com

Journal of Applied Sciences 9 (21): 3836-3842, 2009
ISSN 1812-5654

Large Eddy Simulation of a Rectangular Turbulent Jet in Crossflow

[1,2]E.H. Kali and [2]S. Benmansour
[1]Mechanical Engineering School, USTHB University, P.O. Box 32,
El Alia, 16111, Bab Ezzouar Algiers, Algeria
[2]MoST/LEGI, BP. 53, 38401 Grenoble Cedex 09, France

Abstract: Large eddy simulations are performed to investigate rectangular jets in crossflow. In particular, the jet-to-crossflow velocity ratio influence on flow dynamic and mixing properties is analysed. Conversely to free jets, Kelvin-Helmholtz vortices do not lead to ring structures, they develop at the windward side of the jet. Their shedding frequency is also different. The Strouhal numbers for both mixing layer and wake structures increase with decreasing velocity ratio. Moreover, the upright vortices appear in the wake zone for the case of lower velocity ratio. The near field initiation of the counter-rotating vortex pair formation is demonstrated in the lower velocity ratio case and dominates in the far field. In the higher one, the jet impinges the opposite wall which inhibits the complete development of such structures in the far field. An enhancement of the mixing process in the case of lower velocity ratio as demonstrated by the rapid jet centerline decay of the passive scalar (temperature) seeded in the jet. As a final result, for the dynamics, the overall agreement of the numerical results and those of literature suggests that the jet mixing layer instability is strengthened as the velocity ratio is decreased. While, the wake structures topology is also strongly dependent on the velocity ratio. The mixing process is enhanced by the presence of the counter-rotating vortex pair.

Key words: Large eddy simulation, jet in crossflow, dynamics, mixing

INTRODUCTION

The jet in crossflow (JICF) is defined as a jet interacting with a crossflow. It appears in a variety of technological applications. In the present study, the vortical structures dynamic resulting from this interaction and the mixing properties of a passive scalar (temperature) seeded in the jet are studied. Various research studies have considered the problem of circular jets in crossflow (Smith and Mungal, 1998; Kelso *et al*., 1996; Lim *et al*., 2001; Yuan *et al*., 1999). Fundamental differences have been found with a free jet about the coherent structures dynamic and the mixing properties. For example Yuan *et al*. (1999) found no evidence of existence of ring like vortices in JICF. In the other hand, Smith and Mungal (1998) have reported that the mixing process is enhanced in the case of JICF. These researchers suggest that this enhancement is due to the emergence of a Counter-rotating Vortex Pair (CVP). Note that only few works (Plesniar and Gusano, 2005) have studied the present configuration with a rectangular jet in crossflow. In this case, the results about mixing confirm also the CVP role on mixing enhancement.

FLOW PARAMETERS AND NUMERICAL METHODS

In present simulations, the aspect ratio of the rectangle defined as the ratio of its longer side, l_j, by a shorter one, h_j, is 1.6. Figure 1 shows the computational domain, its size is 15.9 l_j x 6.25 l_j x 7.5 l_j, along the streamwise (crossflow) direction, x and the two transverse directions, y and z. The z axis is the jet direction. Two walls bound the domain in this direction. The Reynolds and molecular Prandtl numbers are $Re=U_j\ lj/\nu = 26{,}000$, with U_j the bulk jet velocity and $Pr = 0.7$, respectively. The

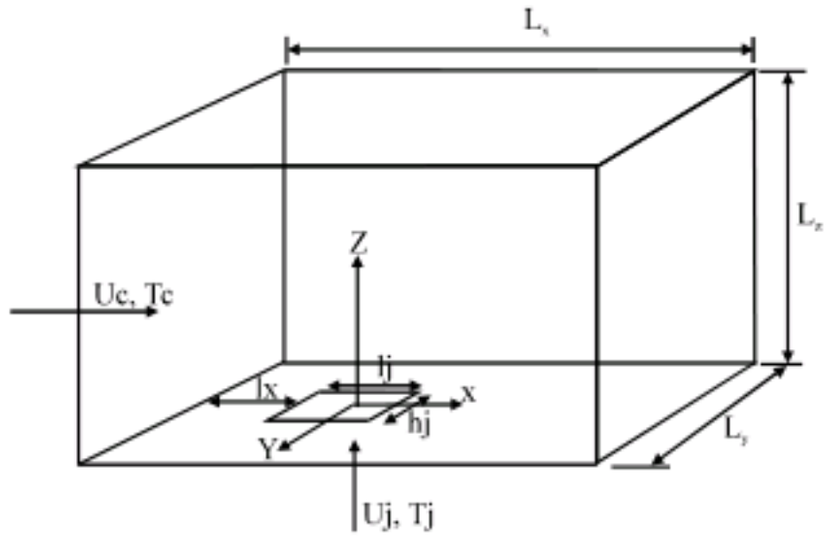

Fig. 1: Geometry of the computational domain

Corresponding Author: El Hadi Kali, Mechanical Engineering School, USTHB University, 16111, Bab Ezzouar Algiers, Algeria
Tel: 00 213 5 56 62 65 61 Fax: 00 213 21 24 79 19

considered jet-to-crossflow velocity ratio values are r = 5 and r = 10. The subgrid-scale (SGS) stress tensor and the SGS scalar flux are respectively modeled by an eddy viscosity type selective structure function model (Lesieur and Métais, 1996) and an eddy diffusivity model with a constant SGS Prandtl number sets equal to 0.6 (Métais and Lesieur, 1992). To provide a realistic jet inlet conditions, a second simulation of a temporally-evolving duct flow is simultaneously ran. The instantaneous profiles are then used as velocity entrance conditions of the jet. Trio_U code (Calvin *et al*., 2002) is used to solve grid-filtered, incompressible Navier-Stokes equations and an advection-diffusion equation for the scalar. The computational domain consists on 224×125×92 points with a local grid refinement applied in the shear layer zone of the jet and on the wall issuing the jet. Space derivatives are centered 4 order for the convection and second order for diffusion. A third order Rung-Kutta scheme is used for time advancement. For pressure-velocity coupling, a Poisson equation is solved to ensure incompressibility at each step of the Rung-Kutta time advancing scheme and SSOR conjugate solver is used for resolution.

RESULTS AND DISCUSSION

Flow dynamic

Global view: Figure 2 shows an instantaneous view of three-dimensional positive Q isosurfaces colored by the value of the vorticity component ω_Z, for the 2 cases, r = 10 and r = 5. Note that the black color corresponds to negative value and the light grey color is for positive. We recall that Q is the second invariant of the velocity gradient tensor and it is well recognized as a good coherent-vortex tracer (Dubief and Delcayre, 2000). The jet is turbulent from the beginning in both cases as shown by the various coherent structures close to the entrance. This is consistent with the downstream fully developed duct. In the r = 10 case, the jet is nearly vertical and impacts the opposite wall as seen in Fig. 2a. In the r = 5 case, the crossflow is strong enough to bend the jet and to avoid the impingement, Fig. 2b. The horseshoe vortex and wake structures, respectively upstream and downstream the jet, are also shown in Fig. 2. These structures are consequences of the interaction between the jet and the crossflow boundary layer. As shown by the zoom in Fig. 2a, the horseshoe vortex is similar to those is found upstream of the bluff bodies. It is due to the deflection of the crossflow around the jet and the stretching of the spanwise vorticity in the crossflow boundary layer. The wake vortices have also their origin in the crossflow boundary layer. These vortices will be discussed in details below.

Jet near field structures: In Fig. 3, isosurfaces of the pressure difference are plotted. They are colored in Fig. 3a and b by $\omega_x+\omega_z$, ω_x and ω_z being, respectively the streamwise and jet-direction vorticity values. The pressure difference is defined as $\Delta p = (p-p_{ref})/\rho\, U_j^2$, where,

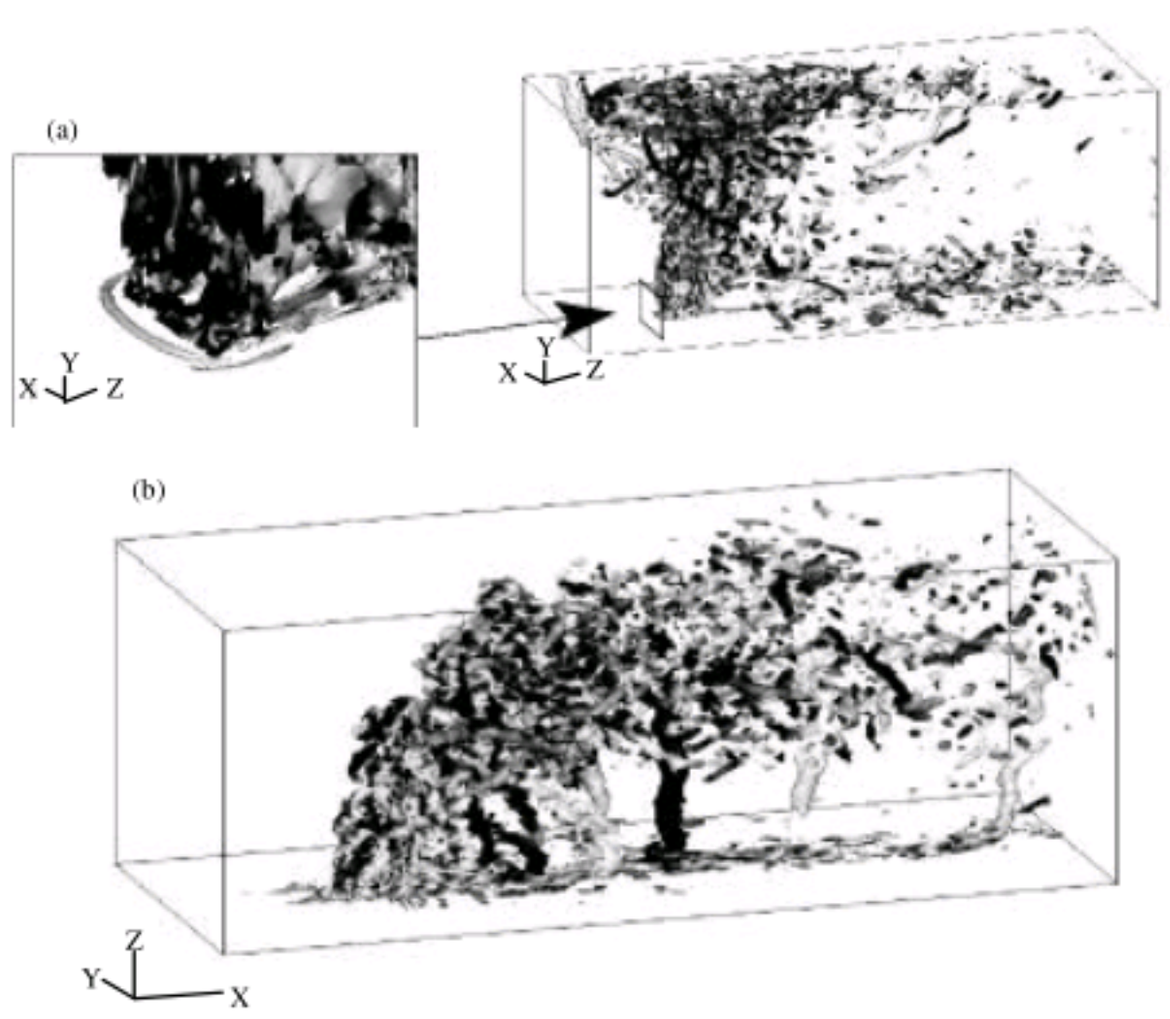

Fig. 2: Isosurfaces of $Q=0.1(U_j/l_j)^2$ colored by the axial vorticity ω_z (a) in the case r = 10 and (b) in the case r = 5

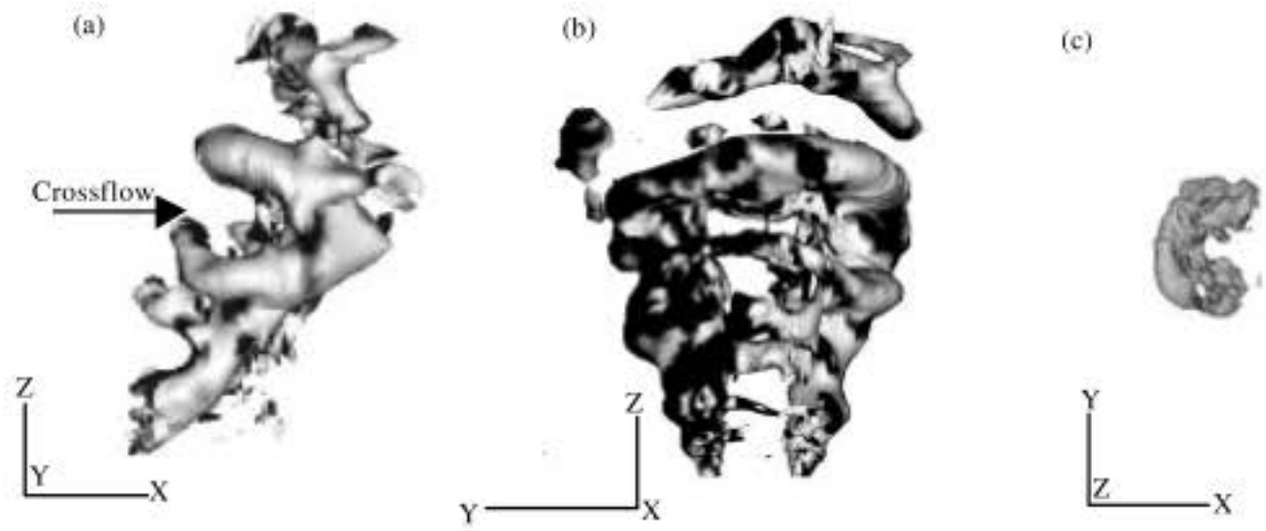

Fig. 3: Isosurfaces of pressure. $\Delta p = (p-p_{crf})/\rho U_j^2$, colored by $\omega_x+\omega_z$ (a) on a lateral view and (b) on the windward view. (c) isolated structure at $z/l_j=3$

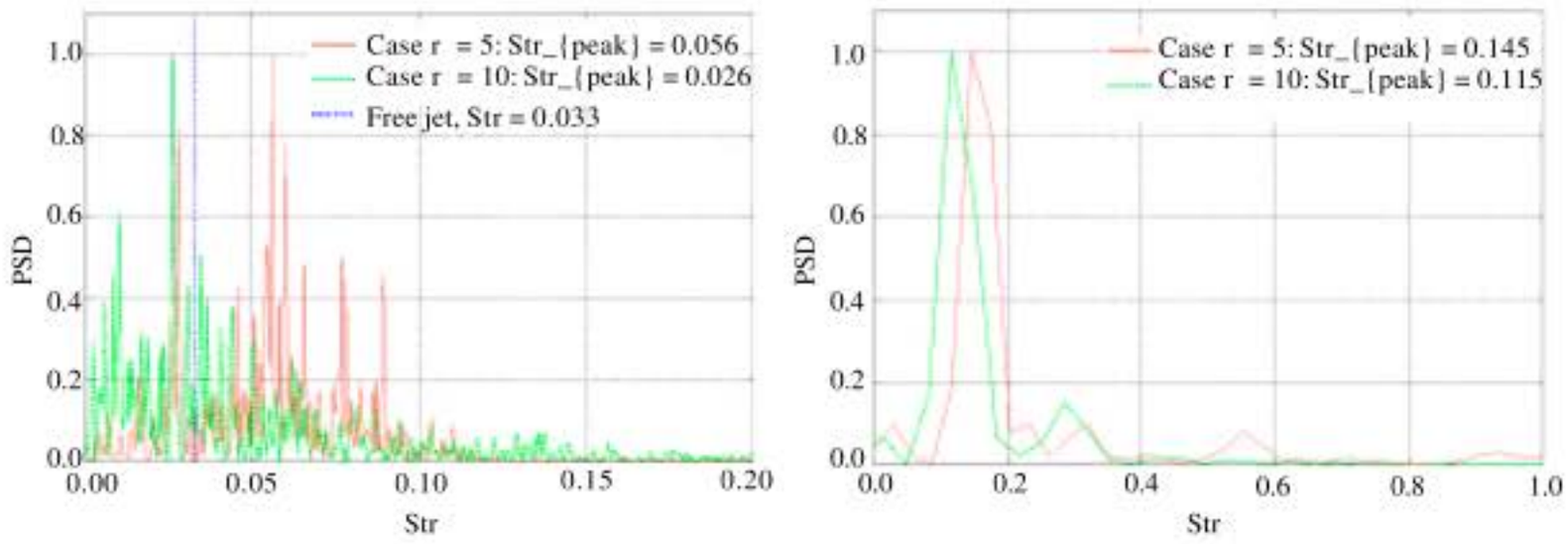

Fig. 4: Velocity power spectral density (a) for the jet mixing layer and (b) for the wake

p_{crf} is the crosstream pressure. The pressure isosurfaces mark the location of the low-pressure cores of vortical structures. They allow to visualize large-scale features in the flow field by filtering the small scale structures. The formation of large-scale coherent structures in the jet mixing layer due to the development of Kelvin-Helmholtz instabilities is seen in the Fig. 3. These structures are wrapping only on the windward side of the jet, Fig. 3a and b. The coherent structures are not well formed on the lee side as shown by Fig. 3c. This is due to the CVP emergence. Indeed, large vortex structures are formed on each side of the jet as seen on Fig. 3a. These structures have a rotation axis close to:

$$\vec{e}_x + \vec{e}_z$$

where $\vec{e}_x$ and $\vec{e}_z$ are the unit vectors in the x and the z direction, respectively.

They lead downstream to the counter-rotating vortex pair (CVP) as shown by the black and light grey colors on the windward view in Fig. 3b. This near-field initiation of the CVP is suggested by various experiments (Smith and Mungal, 1998; Kelso *et al.*, 1996). This pattern of no existence of ring-like vortices such as the case of free jet agrees with the various JICF studies (Lim *et al.*, 2001; Yuan *et al.*, 1999).

For the above reasons the Strouhal number, $Str = f\,\theta/U_c$, is computed at the windward side of the jet. In this expression, f is the frequency, θ the jet mixing layer momentum thickness and U_c is the convective velocity. Figure 4a shows the power spectral density of the jet axial velocity, w, for the two cases. In Fig. 4 the power spectral density is normalized by its maximum. The peak for the case r = 10 corresponds to Str = 0.026 whereas the peak is for Str = 0.056 in the r = 5 case. These values differ from the theoretical one of 0.033 characterizing free jets. This is expected because the presence of the crossflow affects the jet mixing layer instability (Alves *et al.*, 2007). Alves *et al.* (2007) reported that the instability of the mixing layer is fundamentally different in comparison with a free jet even if a extremely large velocity ratio is considered. Indeed, they show that the linear stability results of a JICF are similar as a free jet when the velocity ratio is higher than 270. On the other hand, similar study of the transverse jet shear layer instabilities performed by Alves *et al.* (2008) for large jet to crossflow velocity ratio

(r>4) suggested that the Strouhal number increase with decreasing velocity ratio. These findings are also in agreement with the experimental results of Megerian *et al.* (2007) study for the rang of velocity ratio $4<r\leq 10$.

Wake structures: The wake structures appearing downstream of the jet are due to the closed flow around the jet which imposes an adverse pressure gradient on the wall. This adverse pressure gradient leads to a separation in the boundary layer on each side. There are then eruptions of boundary-layer fluid and formations of wake vortices which are convected downstream.

The velocity ratio effects on the wake is seen by the stretching of these structures along the wall for the higher velocity ratio case as shown by the elongated structures along the wall in Fig. 2a, whereas vertical vortices spanning the space between the jet and the lower wall are shown in Fig. 2b for the lower velocity ratio case. Indeed, it is known that around the jet there exists a region of suction due to jet entrainment. When the jet core is near to the wake (case r = 5) this suction is strong enough to turn up the structures in the vertical direction. In the r = 10 case, the jet core is far from these structures and the effect of suction is weak.

A similar result has been shown by Fric and Roshko (1994). The dynamic of these structures has also been studied in term of shedding frequency. The power spectral density is then constructed from the streamwise (crossflow) velocity mesured downstream the jet, in the boundary layer. The Strouhal number, $Str = f\ h_j/U_{crf}$ is based on the frequency f, the rectangle breadth, h_j and the crossflow velocity, U_{crf}.

Figure 4b, shows the spectrum in the wake, downstream of the jet, for the two cases, r = 10 and r = 5. The peak in the higher velocity ratio case is for Str = 0.115, whereas it is for Str = 0.145 in the other case. There is an increase of the Strouhal number when r decreases.

Indeed in the lower velocity ratio case, the jet is bent and stays close to these structures, Fig. 2b, so they are influenced by the entrainment and accelerated. Conversely, in the higher ratio case, the jet is nearly vertical and it is far from the wake structures, Fig. 2a. Note that these values of the Strouhal number agree with the values computed by Krothapalli *et al.* (1990) in their experimental study of a rectangular JICF. They found that for r = 5, the Strouhal number is 0.15 and diminish to 0.1 for r = 10 in a range of the crossflow Reynolds numbers from 10,000 to 50,000.

Far field structures: The far field is now studied. Large differences between both cases can be observed. Figure 5 shows positive Q isosurfaces colored by the spanwise vorticity ω_y value for the r = 10 case, Fig. 5a and by streamwise vorticity $\grave{u}_x$ value for the r = 5 case, Fig. 5b. The vorticity values are negative for the black color and positive for the light grey color in the corresponding figures. Note that the crossflow direction is from left to right in Fig. 5a. A big horseshoe vortex is seen at the impingement plate. It is formed upstream of the impingement zone and it conserves the rotation direction of the structures impacting the wall.

Figure 5b is a view from the lee side for the r = 5 case. The far field turbulence structures are dominated by the CVP. It is illustrated by the black and light grey colors which show the domination of negative and positive streamwise vorticity, respectively. Note that the main vorticity axis of the CVP is $\vec{e}_x$ in the far field due to the jet curvature.

Scalar mixing: Slices of the scalar field are shown in Fig. 6. Figure 6a, b show a x-z plan at $y/l_j = 0$ for the r = 10 case and the r = 5 case, respectively. In Fig. 6c, the contour slice is in the y-z plan at $x/l_j = 2$. Note that the scalar value varies from zero (white) to one (black). The role played by the coherent structures can be seen. First, at the beginning of the jet, the mixing is initiated by the large Kelvin-Helmholtz vortices on the windward side as shown on the Fig. 6a and b. On the lee side, the CVP emergence allows to mix the hot stream from the jet with the cold stream coming from the lateral side. The major difference between the r = 10 and the r = 5 cases is that there is a strong heating of the upper wall in the first case. This is due to the jet impingement on the wall. The strong heating can be harmful for the materials. In the second case, the crossflow is strong enough to avoid the wall heating. Moreover, in this case, the CVP allows the cold stream engulfment in the jet as shown by Fig. 6c. Thus, no hot fluid spot has been detected after $z/l_j = 3$ in the r = 5 case conversely to the r = 10 case. Further study will be devoted to characterize accurately the impingement condition as a function of the flow parameters.

The mixing efficiency is now investigated by considering the centerline decay of the scalar. Figure 7 shows the mean scalar value along the centerline coordinates. The figure is shown as a log-log plot. Beyond the potential core, the scalar decays roughly as s^{-1}, which is the decay dependence seen in simple jets. This contrasts with the results of Smith and Mungal (1998), for values of r ranging from 5 to 25, who found an initial decay-law of $s^{-1.3}$ which is faster than the present results. This difference is coming from the fact that in Smith and Mungal (1998) study, a top hat velocity profile

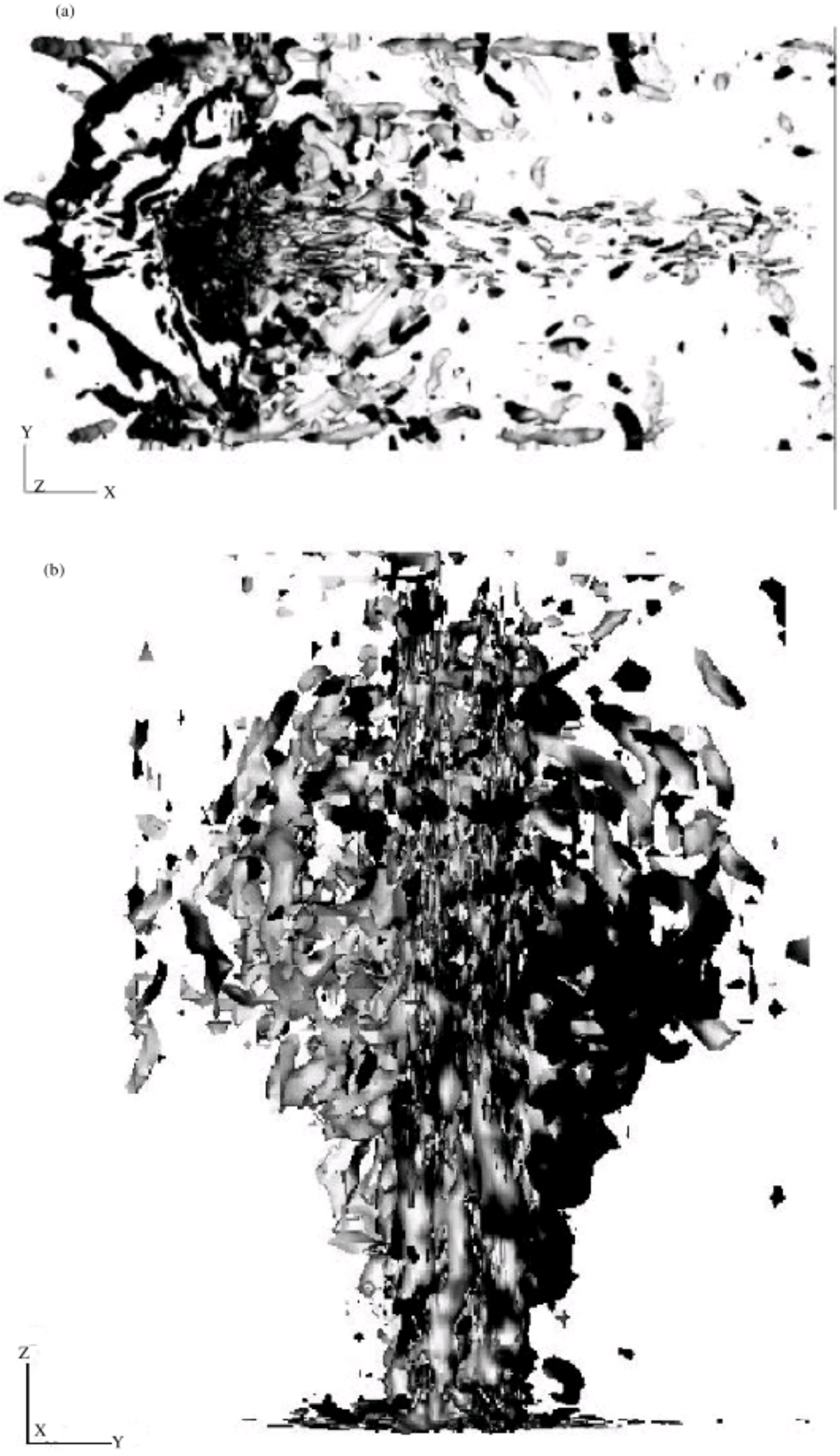

Fig. 5: Isosurfaces of $Q = 0.1(U_j/l_j)^2$, (a) top view of case r = 10 colored by ω_y and (b) lee side view of case r = 5 colored by ω_x.

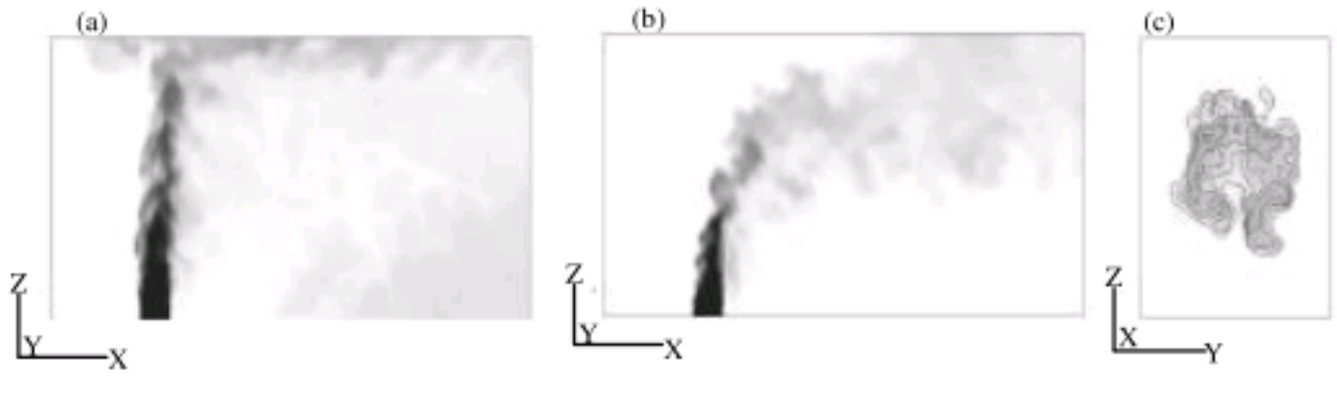

Fig. 6: Slices colored by the scalar field. Plan (x-z) at y/lj = 0 for the (a) r = 10 and (b) r = 5. Plan (y-z) at x/lj = 2 for (c) r = 5

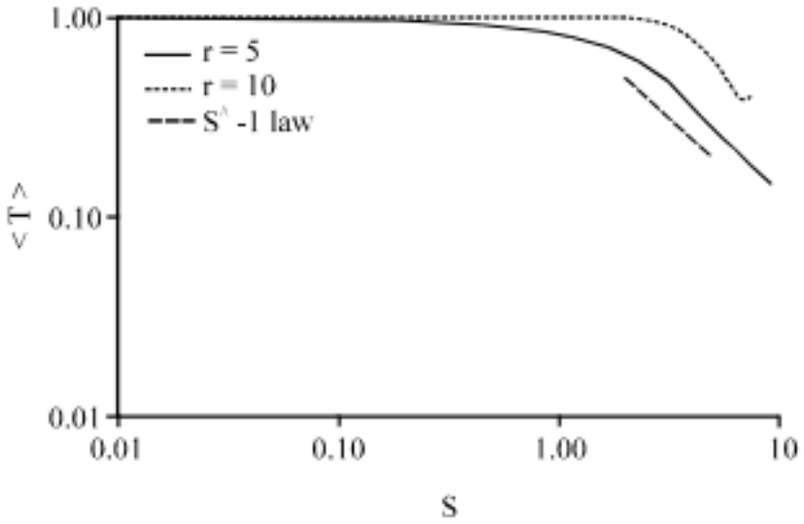

Fig. 7: Centerline scalar decay plotted with downstream distances

is used for defining the jet inlet conditions. Contrary, in the present study fully developed profiles are used for defining the jet inlet conditions. Finally we note that our results show a similar decay rate as those obtained experimentally by Su and Mungal (2004), who uses fully developed conditions at the jet inlet.

CONCLUSION

A numerical investigation of the influence of a velocity ratio on the dynamic and mixing properties for rectangular jet in crossflow has been performed. The dynamic study is focused on the jet mixing layer and the wake structures resulting from the complex interaction between the jet and the crossflow. The Kelvin-Helmholtz structures are found to develop in the windward side of the jet but they do not wrap on the lee side. Their shedding frequency is different of the free jet classical result. Different topology of the wake structures is found for the two cases. In the higher velocity ratio, these structures are stretched along the wall whereas they turn up in the vertical direction in the lower case. There is then an increasing of the passage frequency. The far field of this later case is dominated by the CVP, allowing a mixing enhancement. Thus, the strong heating on the upper wall found for the higher velocity ratio is avoided for this case.

ACKNOWLEDGMENTS

The authors would like to acknowledge the financial support of MESRS/Algeria under Grant PNE-091/2007. Professor Olivier Métais, Doctor Guillaume Balarac of MoST team and CEA-Grenoble are gratefully acknowledged for all the facilities offered and their help.

NOMENCLATURES

f	= Frequency
h_j	= Rectangle breadth
l_j	= Rectangle width
p	= Static pressure
p_{crf}	= Crossflow inlet plane static pressure
Δp	= $p-p_{crf}$
Pr	= Molecular Prandtl number
Q	= Positive Q-criterion
$r=U_j/U_{crf}$	= Jet to crossflow velocity ratio
Re	= Jet Reynolds number
s	= Jet centerline coordinate
Str	= Strouhal number
$< T >$	= Mean temperature
U_{crf}	= Crossflow velocity
U_j	= Bulk Jet velocity
w	= Axial jet velocity
$\vec{e}_x$	= Streamwise (crossflow) unite vector
$\vec{e}_z$	= Axial (jet) unite vector
θ	= Jet mixing layer momentum thickness
ω_x	= Streamwise vorticity component
ω_z	= Axial vorticity component
ν	= Kinematic viscosity

REFERENCES

Alves, L.B., R.E. Kelly and A.R. Karagozian, 2007. Local Stability analysis of an inviscid transvers jet. J. Fluid Mech., 581: 401-418.

Alves, L.B., R.E. Kelly and A.R. Karagozian, 2008. Transverse-jet shear-layer instabilities Part 2: Linear analysis for large jet-to-crossflow velocity ratio. J. Fluid Mech., 602: 383-401.

Calvin, C., O. Cueto and P. Emonot, 2002. An object-oriented approach to the design of fluid. Mechanics Software, 36: 907-921.

Dubief, Y. and F. Delcayre, 2000. On coherent vortex identification in turbulence. J. Turbulence, 11: 1-22.

Fric, T.F. and A. Roshko, 1994. Vortical structure in the wake of a transverse jet. J. Fluid Mech., 279: 1-47.

Kelso, R.M., T.T. Lim and A.E. Perry, 1996. An experimental study of round jets in cross-flow. J. Fluid Mech., 306: 111-144.

Krothapalli, A., L. Lourenco and J.M. Buchlin, 1990. Separated flow upstream of a jet in crossflow. AIAA J., 28: 414-420.

Lesieur, M. and O. Métais, 1996. New trends in large eddy simulation of turbulence. Ann. Rev. Mech., 28: 45-82.

Lim, T.T., T.H. New and S.C. Luo, 2001. On the development of large-scale structures of a jet normal to a cross flow. Phys. Fluids, 13: 770-775.

Megerian, S., J. Davitian, L.S. De B. Alves and A.R., Karagozian, 2007. Transverse-jet shear-layer instabilities Part 1: Experimental studies. J. Fluid Mech., 593: 93-129.

Métais, O. and M. Lesieur, 1992. Spectral large-eddy simulation of isotropic and stably stratified turbulence. J. Fluid Mech., 239: 157-194.

Plesniar, M.W. and D.M. Cusano, 2005. Scalar mixing in a confined rectangular jet in crossflow. J. Fluid Mech., 524: 1-45.

Smith, S.H. and M.G. Mungal, 1998. Mixing, structure and scaling of the jet in crossflow. J. Fluid Mech., 357: 83-122.

Su, L.K. and M.G. Mungal, 2004. Simultaneous measurements of scalar and velocity field evolution in turbulent crossflowing jets. J. Fluid Mech., 513: 1-45.

Yuan, L., R. Street and J. Ferziger, 1999. Large-eddy simulation of a round jet in crossflow. J. Fluid Mech., 379: 71-104.